

# **Initial Experiments with a Scalable Machine Learning Based Approach for Downscaling the MOD16A2 Evapotranspiration Product**

VATSAL JINGAR<sup>1</sup>, Indian Institute of Technology, Delhi

STITIPRAJNA SAHOO<sup>2</sup>, Indian Institute of Technology, Delhi

SIDDHARTH S<sup>3</sup>, Indian Institute of Technology, Delhi

DHARMISHA SHARMA<sup>4</sup>, Indian Institute of Technology, Delhi

SHIVANI A. MEHTA<sup>5</sup>, Indian Institute of Technology, Delhi

AADITESHWAR SETH<sup>6</sup>, Indian Institute of Technology, Delhi

In countries like India which have historically been reliant on rainfed agriculture, the increasing need of water for irrigation to support greater cropping intensity and shifts towards horticulture, has largely been supported through groundwater based irrigation. Cheap electricity has enabled a rapid increase in borewells almost across the country, which to some extent has enabled more equitable access to water than other irrigation approaches like canals, but has also led to groundwater stress in many regions. One way to indirectly estimate groundwater abstraction is to estimate evapotranspiration from cropping areas as a proxy for crop water consumption. Remote sensing based methods have been used to estimate evapotranspiration but existing open data products largely have a low spatial resolution which is not adequate to support local decision making for water use. In this study, we build machine learning methods to develop downscaled data outputs of evapotranspiration at fine spatial scales. Our approach uses satellite data, meteorological variables, and land surface characteristics as input features to obtain field-scale fortnightly time-series of evapotranspiration. We validate the results across multiple geographic locations and also study its correlation with in situ evapotranspiration measurements. We find that our method is not able to accurately match in situ data but is able to successfully provide relative differences in evapotranspiration. We make our trained models available on the Google Earth Engine platform for use by other researchers and practitioners to obtain evapotranspiration outputs for their areas of interest. Our research contributes a scalable and adaptable solution to address the growing demand for fine-resolution hydro-climatic information.

CCS Concepts: • Social and professional topics; • Computing methodologies → Machine learning;

Additional Key Words and Phrases: Downscaling, Evapotranspiration, Water-balance, Random Forests, Regression, Hydrology, Landsat

## **ACM Reference Format:**

Vatsal Jingar<sup>1</sup>, Stitiprajna Sahoo<sup>2</sup>, Siddharth S<sup>3</sup>, Dharmisha Sharma<sup>4</sup>, Shivani A. Mehta<sup>5</sup>, and Aaditeshwari Seth<sup>6</sup>. 2024. Initial Experiments with a Scalable Machine Learning Based Approach for Downscaling the MOD16A2 Evapotranspiration Product. In *ACM SIGCAS/SIGCHI Conference on Computing and Sustainable Societies (COMPASS '24), July 8–11, 2024, New Delhi, India*. ACM, New York, NY, USA, 22 pages. <https://doi.org/10.1145/3674829.3675068>

---

Authors 1 and 2 contributed equally on the ET downscaling methodology, authors 3, 4 and 5 contributed on evaluation on in-situ data, author 6 guided the overall methodology and analysis.

---

Permission to make digital or hard copies of part or all of this work for personal or classroom use is granted without fee provided that copies are not made or distributed for profit or commercial advantage and that copies bear this notice and the full citation on the first page. Copyrights for third-party components of this work must be honored. For all other uses, contact the owner/author(s).

© 2024 Copyright held by the owner/author(s).

Manuscript submitted to ACM

## 1 INTRODUCTION

Evapotranspiration is a key element in the hydrological cycle and represents the water lost as evaporation from bare soil and water bodies and transpiration from plants including crops and trees. Water balance methods often use evapotranspiration estimates, along with rainfall data and runoff models, to estimate groundwater recharge and discharge [5]. Evapotranspiration (**ET**) consists of various components: vegetation transpiration ( $E_c$ ), soil evaporation ( $E_s$ ), and canopy interception evaporation ( $E_i$ ) [5]. A component wise analysis can provide a more precise quantification of water losses from different sources [21], and help with landscape-scale drought monitoring and water requirement assessments [14, 24], precise irrigation scheduling operations [13], and agricultural water allocation and efficient irrigation practices [9], among others to achieve environmental sustainability while also enhancing agricultural production, household income, and nutrition [8].

However, being able to measure actual evapotranspiration at a fine spatial and temporal resolution is currently limited [34]. An open global data product provided as part of the MODIS mission from NASA, called MOD16A2, is available at a coarse resolution of  $500m$ . At this resolution, an ET pixel may contain a mix of different land cover types. Land use and land cover (LULC) classification using satellite systems like Landsat and Sentinel provide outputs at  $30m$  and  $10m$  respectively, and in our work we attempt to downscale the  $500m$  MOD16A2 ET output to a  $30m$  resolution using data from Landsat. This downscaling can then help segregate ET into its various components using knowledge of the LULC classes at a higher resolution.

Our work makes the following contributions:

- Implementation of a Random Forest model that can output a fortnightly time-series of the downscaled ET at a scale of  $30m$  across several Agro Ecological Zones of India using the Google Earth Engine platform, and making it available for scalable use via the platform.
- Analysis of the potential for coarse ET products like MOD16A2 to match in situ measurements. In situ measurements are influenced by site-specific aspects such as localized rainfall and irrigation events which are not easily observable through satellite data, and we explore if our downscaled outputs are able to match these measurements in an absolute manner.

We evaluate our downscaling method in two ways. One, our method is based on an underlying assumption of scale invariance. If the model trained on high spatial resolution features demonstrates accuracy at coarser resolutions, we assume that it can be used at finer resolutions as well. This assumption has been used in several prior studies [16, 7] of downscaling techniques. Our method similarly aims to refine the spatial resolution of ET by capturing local variations in land cover and other factors which are known to influence ET, and we report accuracy results of when this higher resolution ET output is aggregated to coarser regions to match the MOD16A2 output.

Two, we obtain in situ ET data from several ground stations conducting lysimeter measurements operated by the Indian Meteorological Department (IMD) [6]. Although this data is sporadic with substantial missing values, it is perhaps the only source of ET data at scale in India and we evaluate our high resolution ET outputs on this data. We use multi-variate regression to calibrate the downscaled MOD16A2 output using local data (such as temperature, humidity, soil moisture, and precipitation, obtained from a land surface model FLDAS NOAH [33]) and report accuracy results.

We find that the output of our downscaling model when aggregated to coarser resolution is able to match the MOD16A2 output quite well. Visualizations of the high resolution output are clearly able to make out differences across different land use classes like trees, barren land, cropping areas, etc. This makes us confident that our output can be used as a relative ET measure to compare different locations with one another. The output when calibrated to suit local

conditions is however not able to match the in situ data very well. This tells us that being able to match ET in absolute terms continues to be hard, since in situ measurements are likely to be influenced by highly local phenomena which is not observable by the kind of satellite data products we use.

The forthcoming sections outline the background about ET models, the datasets we use, methodology, and results.

## 2 BACKGROUND

### 2.1 Penman–Monteith method

The FAO Penman–Monteith (PM) method ([1]) summarized in equation 1 is well recognized to approximate actual ET from meteorological data:

$$ET_0 = \frac{0.408\Delta(R_n - G) + \gamma \frac{900}{T+273} u_2 \delta e}{\Delta + \gamma(1 + 0.34u_2)} \quad (1)$$

Here,  $ET_0$  is the reference evapotranspiration water volume (in  $mmday^{-1}$ ),  $\Delta$  represents the rate of change of specific humidity with air temperature (in  $PaK^{-1}$ ),  $R_n$  is the net irradiance (in  $MJm^{-2}day^{-1}$ ) which is the external source of energy flux,  $G$  is the ground heat flux ( $MJm^{-2}day^{-1}$ ),  $T$  is the air temperature at 2m( $K$ ),  $u_2$  is the wind speed at 2m height (in  $m/s$ ),  $\delta e$  is vapor pressure deficit (in  $kPa$ ), and  $\gamma$  is Psychrometric constant (where  $\gamma = 66PaK^{-1}$ ).

The MOD16A2 ET algorithm is based on the Penman–Monteith equation and is calibrated based on remotely sensed data for various regions [27]. As non-domain experts, our preference was not to undertake these computations ourselves but rather to utilize existing data products such as MOD16A2. The main challenge that such algorithms face is with the unavailability of base data of various input variables at a high resolution, leaving downscaling as the next viable option.

### 2.2 Related work

We next provide an overview of different methods to produce high resolution ET maps, and their evolution, innovations, and critical gaps. Some works have evaluated the performance of spatial interpolation techniques such as Inverse Distance Weighting (deterministic method) and Ordinary and Universal Kriging (geostatistical method) to produce evapotranspiration estimates using in situ measurements [15]. However, a comprehensive comparison of spatial interpolation methods of environmental variables have typically shown higher accuracy with hybrid interpolation models involving machine learning to also include location-based covariates [22, 4]. Several such models have been developed over recent years to estimate ET using ensemble Kalman Filters [28], artificial neural networks [26], support vector machines (SVM) [31], regression trees [36], and Bayesian model averaging methods [39]).

Given sparse availability of in situ measures, alternative approaches of downscaling coarse resolution evapotranspiration using support vector machines have also been developed [18], along with methods that use high resolution satellite data for downscaling [7]. We adopt a similar approach. Existing work in this area has not attempted to provide trained models that can be used across many climate regions, which is a gap we attempt to fill. We are able to provide trained models to produce a downscaled ET product at a 30m resolution for several agro-climatic regions, in a usable form on the Google Earth Engine (GEE) platform that can be used for hydrological and agricultural use-cases like local water management, irrigation scheduling, and monitoring water management budgets. We opt for a Random Forest model due to its scalability for integration into GEE. All base datasets we use are already available publicly on GEE, making our outputs easily usable by any GEE user.

### 3 DATASET

#### 3.1 MODIS

Evapotranspiration estimates obtained from the Terra Moderate Resolution Imaging Spectroradiometer (MODIS) product, MOD16A2 version 6.1 ([30]), is used as the ET target variable to estimate. The underlying algorithm is based on the Penman-Monteith equation. It produces an 8-day composite dataset at a  $500m$  pixel resolution, where the ET value represents the total Evapotranspiration across the eight days in the composite period.

#### 3.2 Landsat

We use Landsat 8 data provided by the Operational Land Image (OLI) sensor onboard the Landsat-8 constellation operated by the U.S. Geological Survey and NASA. It provides bands related to vegetation types, water presence, land surface temperature, etc. at a resolution of  $30m$ . Landsat imagery captures  $185km$  swaths on its orbit and acquires images of the same location on the Earth approximately every 16 days, which is its *average revisit time* ([25]). The Landsat bands were processed to compute 9 indices, namely Normalized Difference Vegetation Index (NDVI), Soil-Adjusted Vegetation Index (SAVI), Normalized Difference Built-up Index (NDBI), Normalized Difference Water Index (NDWI), Modified Soil-Adjusted Vegetation Index (MSAVI), Normalized Difference Moisture Index (NDMI), and Normalized Difference Infrared Index for Band 7 (NDIIB7), Surface Albedo, Land Surface Temperature (LST), at  $30 m$  resolution for the training and test areas, calculated as shown in table 1. The indices NDVI, SAVI, MSAVI are associated with vegetation cover and NDBI, NDWI, NDMI and NDIIB7 are correlated with water consumption that is reflected from ET processes ([19]).

#### 3.3 NOAH-GLDAS

The Penman-Monteith equation 1 incorporates various meteorological variables such as humidity, air temperature, irradiance, ground heat flux, wind speed and vapor pressure to estimate ET accurately. We also use these variables as input features to downscale ET. These meteorological variables include the rain precipitation rate ( $kgm^{-2}s^{-1}$ ), root zone soil moisture ( $kgm^{-2}$ ), soil moisture ( $kgm^{-2}$ ), canopy surface Water ( $kgm^{-2}$ ), specific humidity, wind speed ( $ms^{-1}$ ), pressure ( $Pa$ ), soil temperature ( $K$ ), base flow droundwater runoff ( $kgm^{-2}$ ), shortwave radiation flux ( $Wm^{-2}$ ), heat flux ( $Wm^{-2}$ ), and air Temperature ( $K$ ). They were extracted from the NASA GLDAS version-2 products also available on GEE [2], and are listed in table 2). These variables are available at a temporal resolution of 3 hours with a spatial resolution of 27,830 meters.

### 4 METHODOLOGY

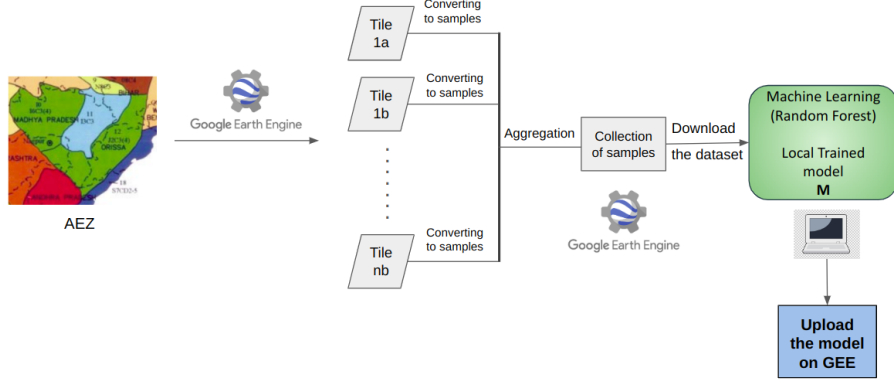
Figure 1a shows all the important components our training and output pipeline. We train our model on the basis of Agro-ecological zones of India (division shown in figure 3) classified as per [12]. These zones provide a meaningful way to characterize specific environmental and agricultural characteristics of different regions. For each zone, we choose all the tiles corresponding to tiles of Landsat 8 satellite images. For all such regions inside the AEZ, we select the dates on which the Landsat and climatic features are both available. Further, the images are brought to same resolution and flattened to generate the samples as shown in figure 1b. Finally, we merge the datasets of adjcent AEZs; we call this collection as a cluster of AEZs and build per-cluster models.

Landsat Index	Formula	Bands	Reference
NDVI	$\frac{NIR - R}{NIR + R}$	NIR: Band 5, R: Band 4	[29]
SAVI	$\frac{NIR - R}{NIR + R + L} (1 + L)$	$L = 0.5$ , NIR: Band 5, R: Band 4	[37]
NDBI	$\frac{SWIR - NIR}{SWIR + NIR}$	SWIR: Band 6, NIR: Band 5	[37]
NDWI	$\frac{Green - NIR}{Green + NIR}$	Green: Band 3, NIR: Band 5	[37]
MSAVI	$\frac{2 * NIR + 1 - \sqrt{(2 * NIR + 1)^2 - 8 * (NIR - R)}}{2}$	NIR: Band 5, R: Band 4	[23]
NDMI	$\frac{NIR - SWIR1}{NIR + SWIR1}$	NIR: Band 5, SWIR2: Band 7	[35]
NDIIB7	$\frac{NIR - SWIR2}{NIR + SWIR2}$	NIR: Band 5, SWIR2: Band 7	[10]
Surface Albedo	$((0.356 * B1) + (0.130 * B2) + (0.373 * B3) + (0.085 * B4) + (0.072 * B5) - 0.018) / 1.016$	B1: Band 1, B2: Band 2, B3: Band 3 B4: Band 4, B5: Band 5	[32]
LST	$K_1 * BT + K_2$	BT: Temperature Band 10 $K_1 : 0.00341802, K_2 : 149.0$	[29]

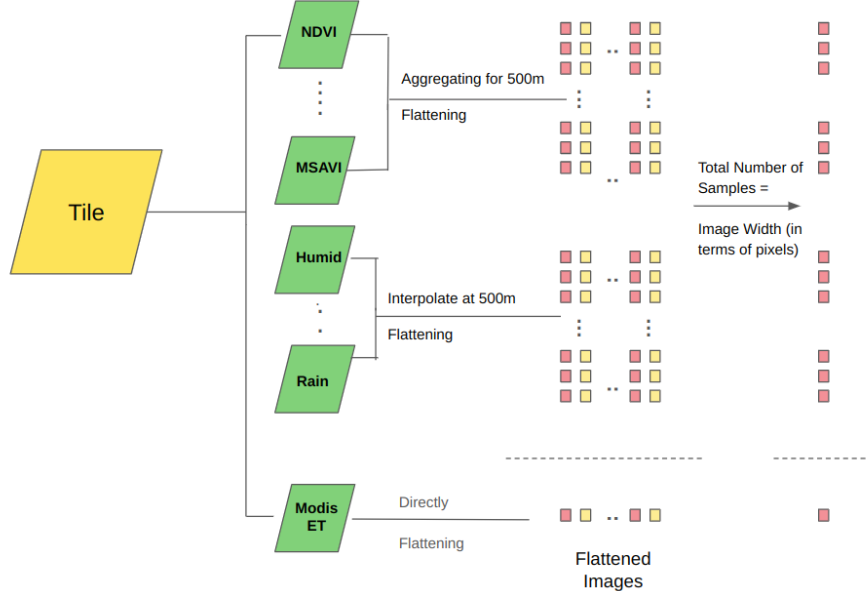
Table 1. Formula for calculating Landsat indices used in the random forest model to estimate ET

Climatic Variable	Band
Rain precipitation rate	Rainf_tavg
Root zone soil moisture	RootMoist_inst
Soil moisture	SoilMoi0_10cm_inst
Canopy surface water	CanopInt_inst
Average Surface Skin Temperature	AvgSurfT_inst
Specific humidity	Qair_f_inst
Wind speed	Wind_f_inst
Pressure	Psurf_f_inst
Soil Temperature	SoilTMP0_10cm_inst
Base flow groundwater runoff	Qsb_acc
Net Short wave radiation flux	Swnet_tavg
Net Long wave radiation flux	Lwnet_tavg
Heat flux	Qg_tavg
Sensible heat net flux	Qh_tavg
Latent heat net flux	Qle_tavg
Downward short wave radiation flux	SWdown_f_tavg
Air temperature	Tair_f_inst

Table 2. The climatic variables that are used in the Random Forest Model, sourced from NOAH-GLDAS



(a) Sampling tiles for multiple dates for a particular AEZ. We choose two different tiles for each date (when Landsat is published).

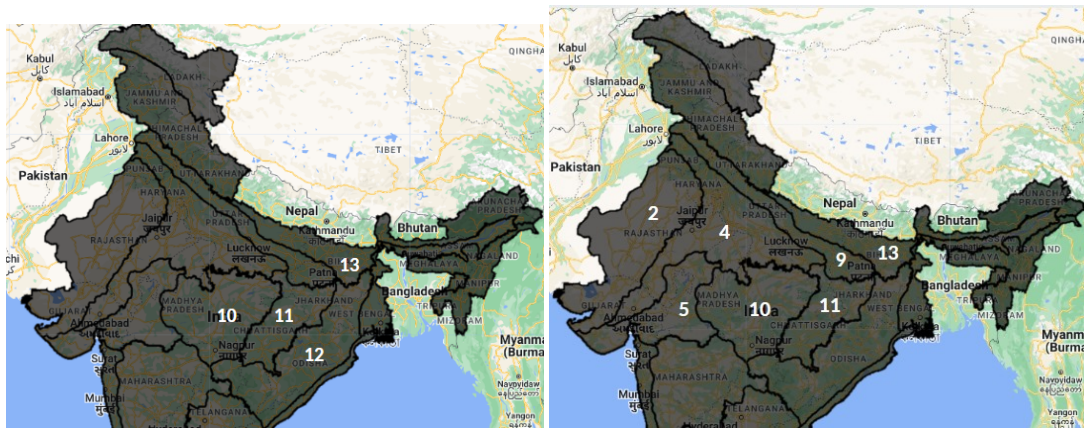
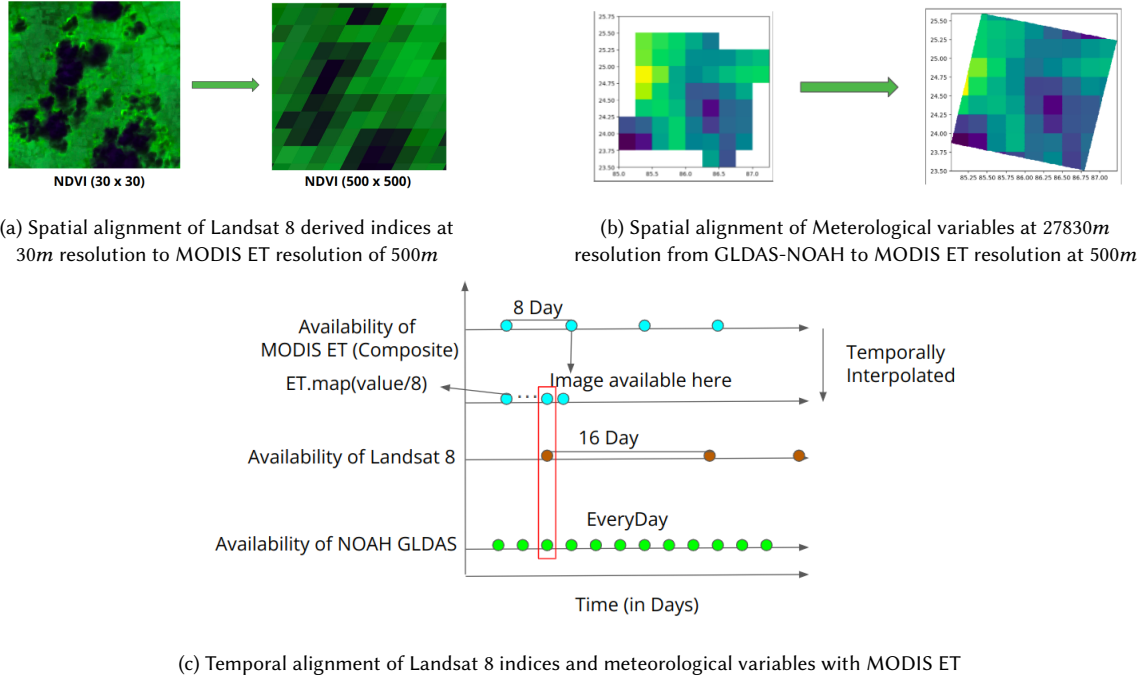


(b) Generating a dataset corresponding to one tile for one particular date

Fig. 1. Pipeline for Dataset Extraction and Training the Model

#### 4.1 Data Preprocessing

The selected images of GLDAS NOAH and Landsat 8 are filtered to match the dates with MODIS ET images as shown in figure 2c. Landsat 8 and GLDAS NOAH images whose acquisition date comes within the 8-day composite window of corresponding MODIS images are selected. The ET value obtained from this MODIS image is considered as the estimate of ET for the corresponding dates of Landsat indices and meteorological variables, since MODIS provides 8-day composite ET values for this window. The selected images are then preprocessed for the computation of Landsat derived



indices (as in table 1) and Meteorological variables. The target ET value provided as input to the random forest model is the  $\frac{1}{8}$ <sup>th</sup> of the value of the 8-day composite ET from MODIS [20], for tiles where the Landsat and GLDAS-NOAH acquisition dates lie within the 8-day period. The values of ET in all the graphs and experiments in our study are in units of 0.1mm/day [30].

For alignment of input features with ET for training purposes, we choose the spatial characteristics of MODIS images as the common reference system and align input features to it, according to figures 2a and 2b. To match the spatial resolution of Landsat 8 indices which are originally at 30m with the resolution of target MODIS ET of 500m, the first step is aggregation. There are three popular aggregation methods, namely averaging, median, and central-pixel sampling, each of which involves producing a single value over a region of  $n \times n$  (here,  $n = 500m$ ). The averaging method is considered to be most suitable for aggregating remotely sensed data ([3]). We therefore use average aggregation to upsample the Landsat 8 images by computing the mean value of all 30m pixels of Landsat that are located within each 500m pixel of MODIS ET. This is followed by reprojection of the Landsat 8 image to match the Coordinate Reference System of the corresponding MODIS image.

For similarly using meteorological variables which are originally at 27,830m and need to be matched with target MODIS ET at 500m, we resample the GLDAS NOAH images to a 500m resolution by converting each pixel of 27,830m to multiple pixels of 500m each, and then reproject them to match the Coordinate Reference System of the corresponding MODIS images.

#### 4.2 Train and Test sets

Post the temporal and spatial alignment of the Landsat 8 and NOAH GLDAS images with MODIS ET as per figure 2, each pixel of the input images are available at a resolution of 500m. Described next is the process we follow to identify spatially and temporally diverse samples for machine learning.

India experiences three primary agricultural seasons, namely Kharif (Jul-Oct), Rabi (Nov-Feb), and Zaid (Mar-Jun). To capture variations in ET across these seasons, we sample training points uniformly from each season of a particular year. We sample 200 pixels from each input tile, and as there are roughly six tiles that satisfied temporal alignment conditions per season, we sample 1200 pixels per season for a year. The total number of sampled pixels in terms of the number of tiles are:

$1200 \times 3(3 \text{ seasons per year}) \times k(\text{Number of Tiles chosen}) \times l(\text{Number of AEZs}) \times 6(6 \text{ images obtained for 6 years: 2016-21}) = 21600 \times k \times l$ . We assume that tiles chosen from each zone are approximately equal.

We uniformly sample two hundred thousand points out of these to constitute the training data for a cluster of AEZs. We chose this method of sampling to limit the number of samples in a dataset but to also have diversity in the dataset. Sampling many pixels for a specific date was not useful as most of them showed similar characteristics.

To validate our model, we use the scale invariance assumption [16] explained in section 1 to aggregate the 30m downscaled ET outputs to 500m pixels. We conduct an evaluation under different settings. Let  $AEZ_{clusterpart}$  be the AEZ whose data is used in training a downscaling model and  $AEZ_{others}$  be other AEZs whose data is not used for training. From these AEZs, we select two sets of locations each for validation. For each of the two sets of locations, Landsat 8, NOAH-GLDAS, and MODIS-ET images are extracted for a year other than the years used for training, and from all three seasons (Section 4.1). Choosing different AEZs and years provide a stronger criteria for evaluation to check whether the trained models are generalizable. These different evaluation settings are described as: (1) *Validation Region 1*: Regions of  $AEZ_{clusterpart}$ , and (2) *Validation Region 2*: Region from  $AEZ_{others}$ . 20,000 points were uniformly sampled for each of these sets of regions and used to assess the model's accuracy at a 500m resolution.

#### 4.3 Model development

We train a random forest model on the collection of training points and store the random forest model corresponding to each AEZ cluster. Earlier research (Section 2.2) on downscaling ET have shown a good accuracy with using random

forest or SVM classified [31, 4]. Additionally, Random Forest models can be used directly on Google Earth Engine, making it feasible to generate outputs at scale. Trained models can thus be used to produce downscaled ET outputs corresponding to any region belonging to the corresponding cluster on which it is trained.

The models are validated for all the validation regions as discussed in Section 4.2. We perform grid search on the set of hyperparameters (number of estimators and depth of each estimator in the random forest) and the best performing hyper-parameter tuned random forest model is stored for the cluster as an asset in GEE for future use.

#### 4.4 Calibration

Calibration is performed as the last step to further align the downscaled ET output with in situ data from IMD. This is done using a multi-variate linear regression model. The parameters used for calibration are the downscaled ET, indices calculated using Landsat 7, and climatic variables gathered from FLDAS NOAH [33] (temperature, humidity, soil moisture, and precipitation). We had to train a new model on Landsat 7 for comparison with the IMD data since the bulk of this in situ data was available during the 2000s when Landsat 8 was not operational [11]. This is described in more detail in the next section.

### 5 IMPLEMENTATION

The algorithm is implemented in Javascript on Google Earth Engine (GEE) and is available to generate  $30m$  resolution ET for any region of India. The source code is available on github and outlines the following steps:<sup>1</sup>

- (1) Export training data and validation data in the form of CSV files to Google Drive, from Google Earth Engine.
  - (a) Extract Landsat 8, NOAH-GLDAS and MODIS-ET images filtered for the specified years on which we want to train. These years are provided as configurable input parameters.
  - (b) Clip the images for the geometries of primary regions (configurable).
  - (c) Temporally align input and MODIS-ET by ensuring that the input data falls within the composite 8-day interval of the MODIS-ET acquisition, achieved by date difference checking.
  - (d) Aggregate to  $500m$  resolution (using mean aggregation) and reproject Landsat 8 images to MODIS-ET projection. Resample NOAH-GLDAS images to  $500m$  scale and reproject to match MODIS-ET projection.
  - (e) Compute the indices listed in table 1, and add the climatic variables listed in Section 3.3 and MODIS-ET values for the corresponding pixels to Landsat images.
  - (f) Sample a subset of pixels (as described in Section 4.2) from the selected Landsat images and export the pixels (in form of a tuple of input features and ET values) to a CSV file in Google drive. The filenames are configured as input. Remove the samples with any null values. Divide the values of ET by 8 to get daily values, as explained in Section 4.1 for temporal alignment.
- (2) Train the Random Forest Model locally. Due to limitations of GEE in terms of the size of the training dataset, hyperparameter tuning and analysis was performed locally.
  - (a) The RandomForestRegressor (with tuned hyperparameters) from sklearn is trained on the training data downloaded from Google drive.
- (3) Export the trained Random Forest Model to GEE as an asset.
  - (a) Serialise the trained RandomForestRegressor to a list of strings (where each string represents a decision tree)
  - (b) Convert the list of strings to a feature collection and export it to GEE as an asset.

---

<sup>1</sup>github repository for ET Downscaling-GEE and for ET Calibration-GEE

State	Average Annual rainfall (in mm)	Forest cover (in %)	AEZ
Madhya Pradesh	1086.25	25.14	10
Jharkhand	1444.8	29.76	11
Chhattisgarh	1309.6	41.21	11
Uttar Pradesh	914.4	6.15	13
Bihar	1512.7	7.84	13
Odisha	1420.8	33.50	12

Table 3. Average annual rainfall (in 2021) and percentage forest cover (2021) of the chosen states in India

- (4) Use the trained Random Forest Model asset to output  $30m$  downscaled ET on GEE
  - (a) Extract Landsat 8 and NOAH-GLDAS images for the required geometry of which we require the downscaled ET product, and filter for the dates on which we want to produce ET.
  - (b) Compute the indices as in table 1
  - (c) Resample NOAH-GLDAS images to  $30m$  and reproject them to match Landsat 8. Add the meteorological variables as outlined in Section 3.3 to corresponding pixels in the input images.
  - (d) Load the trained Random Forests model and use this to infer ET at  $30m$  resolutions.
  - (e) Visualise the  $30m$  ET output on GEE maps for any specified geometry.

## 6 RESULTS

We next show the results of downscaling ET for a few AEZs: Table 3 - AEZ 10 (mostly Madhya Pradesh (Latitudes  $21.6^\circ N$  to  $26.3^\circ N$ , Longitudes  $74.9^\circ E$  to  $82.48^\circ E$ )), AEZ 11 (mostly Jharkhand (Latitudes  $21.57^\circ N$  to  $25.14^\circ N$ , Longitudes  $83.20^\circ E$  to  $87.58^\circ E$ ), mostly Chhattisgarh (Latitudes  $17.55^\circ N$  to  $24.33^\circ N$ , Longitudes  $79.5^\circ E$  to  $84.91^\circ E$  )), AEZ 13 (mostly Uttar Pradesh (Latitudes  $23.52^\circ N$  to  $31.28^\circ N$ , Longitudes  $77.3^\circ E$  to  $84.39^\circ E$  ), mostly Bihar (Latitudes  $24.20^\circ N$  to  $27.31^\circ N$ , Longitudes  $83.19^\circ E$  to  $88.17^\circ E$  )), and AEZ 12 (mostly Odisha (Latitudes  $17.31^\circ N$  to  $22.31^\circ N$ , Longitudes  $81.31^\circ E$  to  $87.29^\circ E$  )). The average rainfall [38] and percentage of forest cover [17] in these states are also shown in table 3. Our experiments are based on these states to include the diversity in cropping areas, land cover types, and rainfall, as these states embody a broad spectrum of climate and land-use variations. We first show an evaluation when separate models are trained for each AEZ, and then show the usefulness of combining multiple AEZs together to form a *cluster* and train per-cluster models.

### 6.1 Single-AEZ Models

We sample points as explained in Section 4.2. The results of the individual AEZ-wise random forest models are shown in figure 11 and the RMSE, NRMSE and R2 scores mentioned in table 4

AEZ	Single-AEZ			Multi-AEZ		
	RMSE	NRMSE	R2	RMSE	NRMSE	R2
10	4.65	0.39	0.87	4.62	0.39	0.87
12	9.45	0.48	0.70	9.07	0.46	0.70
11	6.39	0.39	0.82	6.41	0.41	0.83
13	7.89	0.43	0.65	7.01	0.43	0.67

Table 4. RMSE and R2 scores for validation data of the Single-AEZ random forest models and Multi-AEZ model trained on 2016-2021 and validated for 2022. The ET is measured in units of  $0.1\text{mm/day}$

Based on the graphical analysis of plots in figure 11, it is evident that the random forest model, optimized by hyperparameter tuning, shows favorable performance in the case of points sampled from AEZ 10. However, it performs relatively poorer for values greater than  $5\text{mm}$  in AEZ 11 and AEZ 12. To address this, and to avoid training separate models for each AEZ, we tried to combine adjacent AEZs together into an AEZ cluster and also include more points with ET values  $> 5\text{mm}$ .

## 6.2 Multi AEZ Model

Building separate models for each AEZ can be computationally expensive and also lead to challenges with model management. Combining neighbouring AEZs together could potentially address these concerns and also improve the diversity in the dataset.

We therefore experimented with a multi-AEZ model by pooling training data from various neighboring AEZs. The training dataset now includes data points collected from the states of Bihar, Madhya Pradesh, Jharkhand, Chhattisgarh, and Odisha (thus combining multiple AEZs - 10, 11, 12, and 13) for the years 2016-2021. This pooled training data was used to train a random forest model and validated for points sampled from individual zones in the year 2022. The results on validation data for individual AEZs are mentioned in table 4, and the scatter plots for validation datasets shown in figure 4.

As observed from the results, the performance of the multi-AEZ model is slightly better than the single-AEZ models, and also more advantageous with having to maintain a single model only. We therefore use this strategy for the final calibration step.

## 6.3 Leave-One-Out Validation

Since the multi-AEZ model was preferable, we proceed with evaluating it using a further Leave-One-Year-Out validation strategy to rigorously assess the performance of the model across a 6-year temporal span. Here, we withhold one year's data as the validation set while utilizing the remaining years for training the random forest model. By iteratively repeating this process for each individual year, we aim to evaluate the model's robustness to generalize across different years. We performed the experiment for all the study AEZs and found that the results were consistent across the years, showing the robustness of the model.

## 6.4 Performance on different LULC:

Land Use Land Cover (LULC) maps of an area can help us understand if our downscaled ET outputs are different over the different LULC classes of Forests (land covered with dense trees and undergrowth), Crops (areas used for farming and cultivation of crops), Built-up (high concentration of buildings and other infrastructures), and Shrubs-scrubs (areas dominated by shrubs and scrub vegetation). We compare the performance of the Random Forest model for these classes by identifying roughly LULC-homogeneous regions of area approximately  $2\text{ km} \times 2\text{ km}$ . These regions were sampled from across AEZs 11 and 12 since these AEZs cover a wide variety of regions covering all the 4 LULC classes. The scatter plots of the predicted ET values vs actual ET values for the 4 types of LULC are shown in figure 5. We find that the R<sup>2</sup> values of data points sampled from forest regions is quite low in compared to the R<sup>2</sup> values of data points from cropping and built-up regions. This helps us understand the shortcomings of our model and we discuss this further in Section ??.

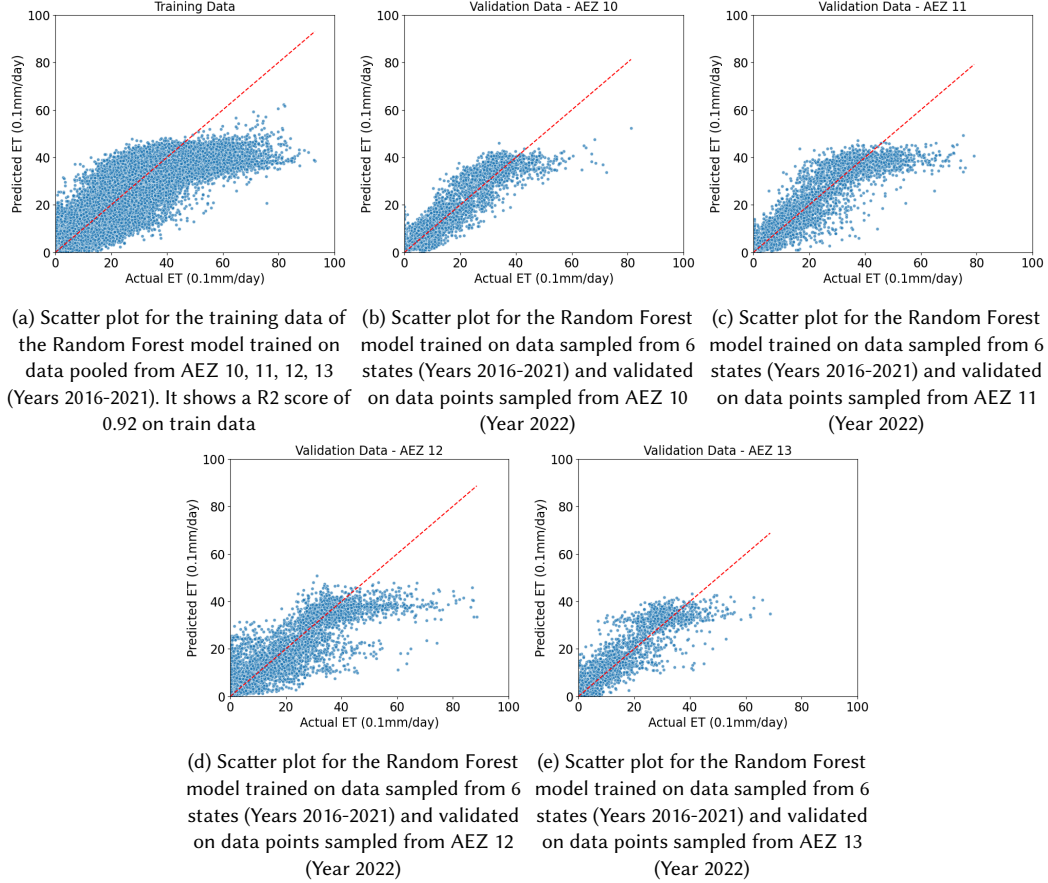


Fig. 4. Scatter plots of train data and validation data for the Multi-AEZ model. x and y axis show ET in units of 0.1mm/day

## 6.5 Visual validation

As a demonstration of our method, we show visualisations of the downscaled ET output at 30m resolution alongside the MODIS ET product at a 500m resolution, and the maps of that area. We can observe the relationship between land cover types and downscaled 30m ET in figures 6 and 7. In general, the ET values are higher on forest pixels and lower for built-up regions, as expected. The output also clearly distinguishes between distinctive features of forests, crops, roads, etc. shown in figure 6, whereas the MODIS ET product does not give us any clear information about the ET distribution within the area. This comparison implies that the downscaled outputs are able to learn relevant relationships and should be able to provide relative ET comparisons at the very least.

The 30m output for larger regions of approximately 50 km × 75 km also aligns well with the MODIS ET products, as well as the satellite maps, as shown in figure 7. This further validates our model and its capability to distinguish across different land use types.

We also show scatter plots for our model's ET output vs MODIS ET aggregated over different LULC classes in the small regions of 2 km × 2 km, in figure 8. We also show in figure 6g four different pixels A,B,C, and D belonging to

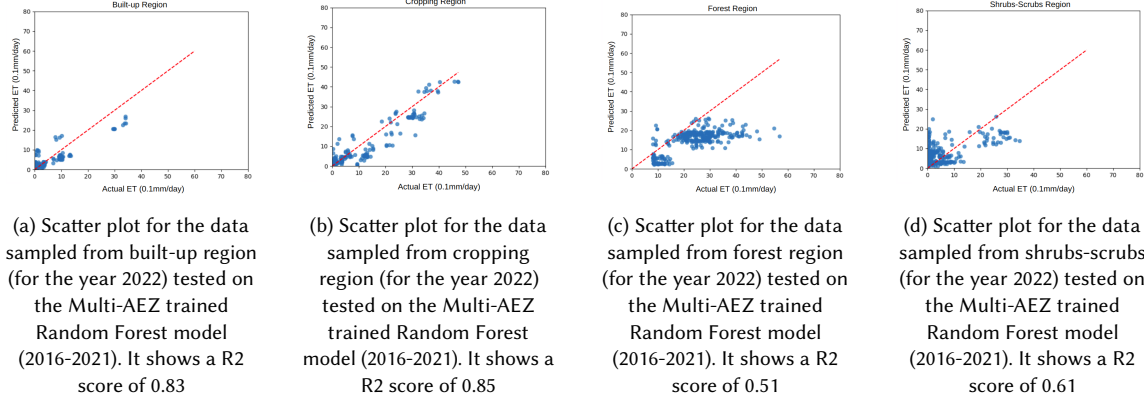


Fig. 5. Scatter plots of train data and validation data for the Multi-AEZ trained Random Forest model on different LULC data. x and y axis show ET in units of 0.1mm/day

different LULC classes shown in figure 9a, and the time series graphs of the downscaled ET output at these pixels, in figure 9b. As observed from the time series plots, the alignment between the downscaled ET time series and MODIS ET time series further demonstrates the accuracy of the random forest model. This suggests that the model is successful in capturing the trends, seasonality, and other patterns present in evapotranspiration data and can be used for relative comparison at the very least.

## 6.6 Calibration

We next proceed to validate the downscaled output against in situ data obtained from IMD. The IMD data is sparse and available as daily measurements in substantial quantity for only a few locations. These locations are spread across AEZs 2 (Dantiwada, Jodhpur), 4 (Durgapura, Jhansi, New Delhi, Rajkot), 5 (Anand), 9 (Varanasi, Bikramganj), 10 (Bhopal), 11 (Raipur), and 13 (Lucknow). Further, IMD data was available mostly during the period in 2000s when Landsat 8 was not operational, and we therefore trained a new multi-AEZ model using Landsat 7. Table 5 shows the model performance for different AEZs, and is mostly in line with the models trained on Landsat 8.

AEZ	Multi-AEZ		
	RMSE	NRMSE	R2
2	25.74	0.54	0.804
4	36.28	0.516	0.735
5	36.33	0.484	0.847
9	37.196	0.399	0.666
10	35.968	0.346	0.87
11	37.616	0.3015	0.889
12	46.29	0.294	0.832
13	36.373	0.284	0.838

Table 5. Statistics for Multi AEZ model trained using Landsat-7 features (required for calibration) on AEZ 2, 4, 5, 9, 10, 11, 12 and 13 and then validated on each of the AEZs one by one. Training performed on 2016-2021 and validated for 2022.

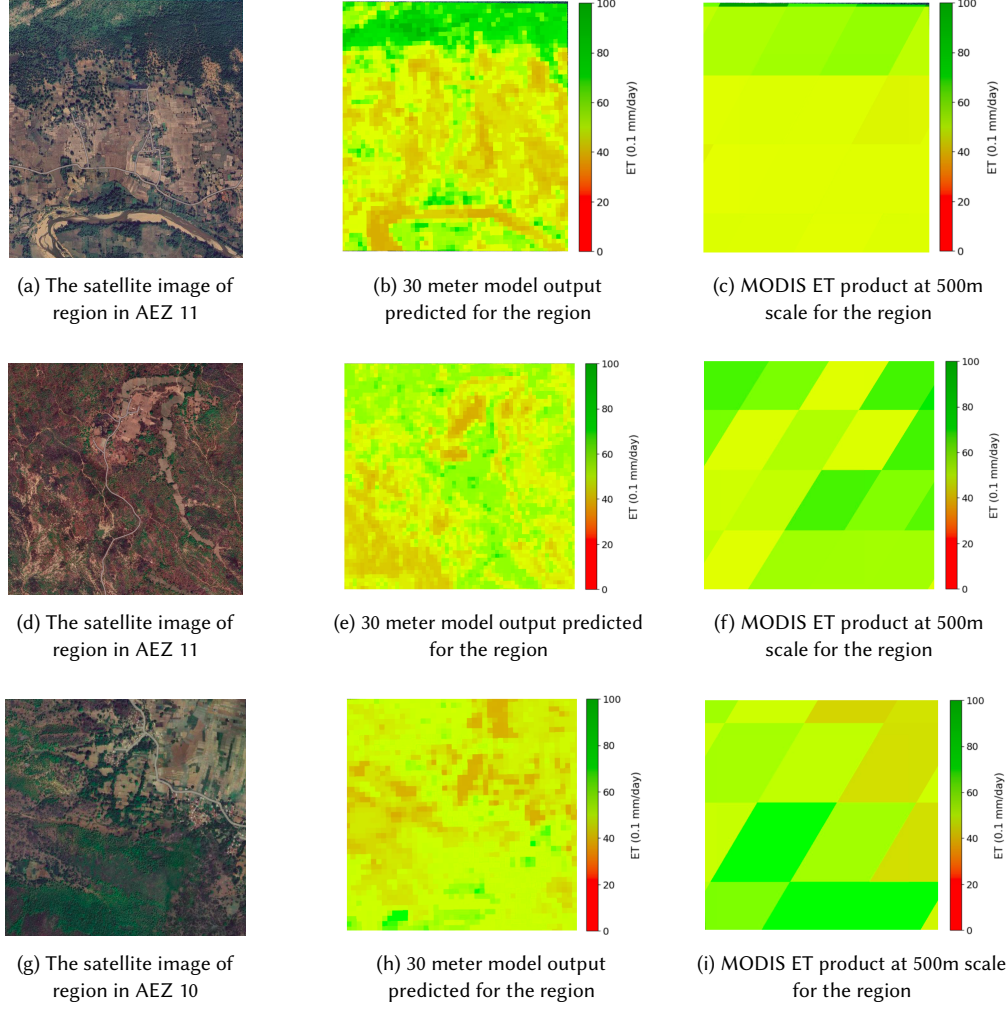


Fig. 6. Visualisation of 30 meter resolution ET product predicted by the trained Random Forest Model for regions from AEZ 10 and 11 of area  $2 \text{ km} \times 2 \text{ km}$  against satellite images and MODIS ET products.

Rather than directly evaluate the downscaled ET against in situ measurements, it is well known that calibration of global products is often needed to fit them to local and regional settings. We conduct two types of calibration using multi-variate linear regression: one which only includes meteorological variables in addition to the downscaled ET to predict in situ measurements, and one which also includes Landsat 7 features. Since most meteorological variables are available at a coarse resolution of several kilometers, including the Landsat variables may help the calibration be sensitive to local events. For meteorological variables, instead of reusing GLDAS NOAH again at this step, we use a higher resolution product, FLDAS [33]. The linear regression coefficients and standard errors for various input features are shown in table 6 (Only FLDAS variables used for calibration). Results of the RMSE, NRMSE, R<sup>2</sup>, and Pearson correlation coefficients, computed before and after the calibration, are also given in table 6. The resulting graphs for all the locations

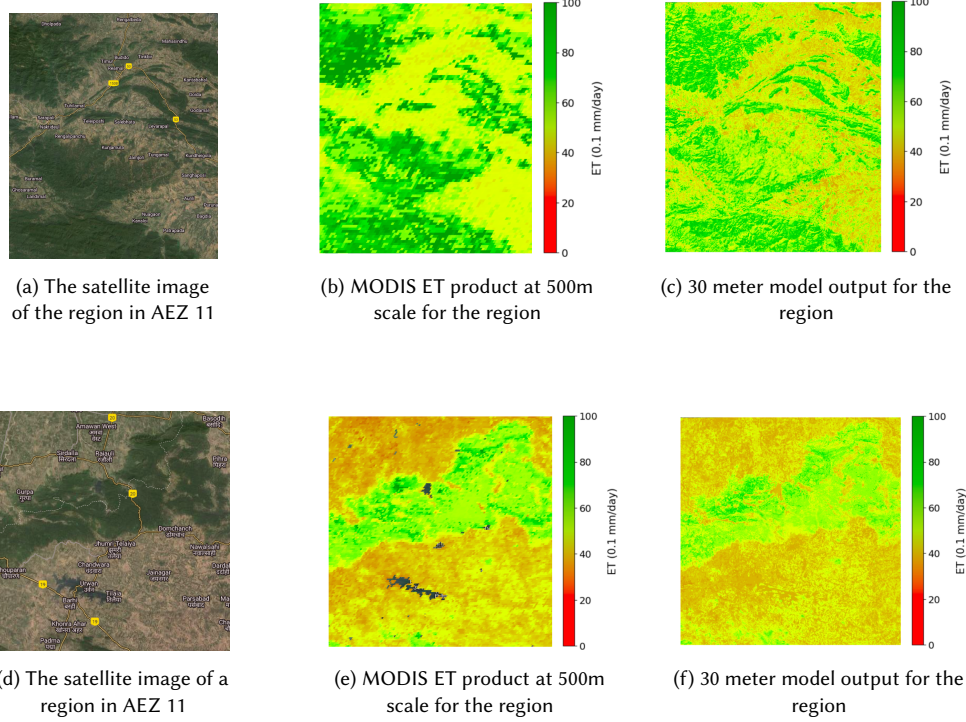


Fig. 7. Visualisation of 30 meter resolution ET product predicted by the trained Random Forest Model for regions from AEZ 11 of area  $50 \text{ km} \times 75 \text{ km}$  against satellite images and MODIS ET products.

are shown in figure 10. 3 locations, namely Bikramganj (AEZ-9), Varanasi (AEZ-9) and Jhansi (AEZ-4) could not be calibrated because of a lack of adequate data and hence were omitted. We also ran an AEZ-level calibration by combining together data of all locations in the same AEZ. We experimented with other models as well, including linear regression with ridge and lasso regularization, and Random Forest and Support Vector machine based methods. In general, we found that AEZ level models performed better than individual location based calibration models, and models using both FLDAS and Landsat features fared somewhat better than models with just FLDAS features.

However, our conclusion from this exercise was that even despite such calibration, we were not able to successfully match the downscaled ET output with in situ data. The R<sup>2</sup> values remained low. This leads us to believe that being able to produce field level ET estimates remains an open challenge; in the absence of high resolution meteorological data, and the gaps in even 30m Landsat data to capture local events, being able to estimate actual ET is challenging. However, the promising ability of the downscaled ET output to differentiate across different LULC classes leads us to believe that relative differences in ET may still be feasible to achieve.

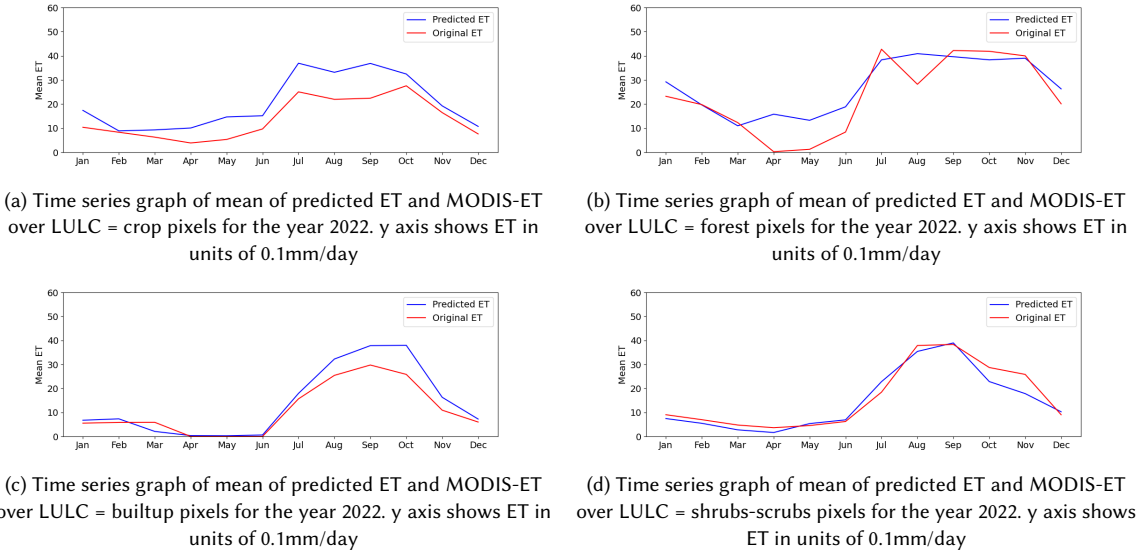


Fig. 8. Time series graphs of Evapotranspiration over different  $2\text{km} \times 2\text{km}$  regions, each covering a specific LULC.

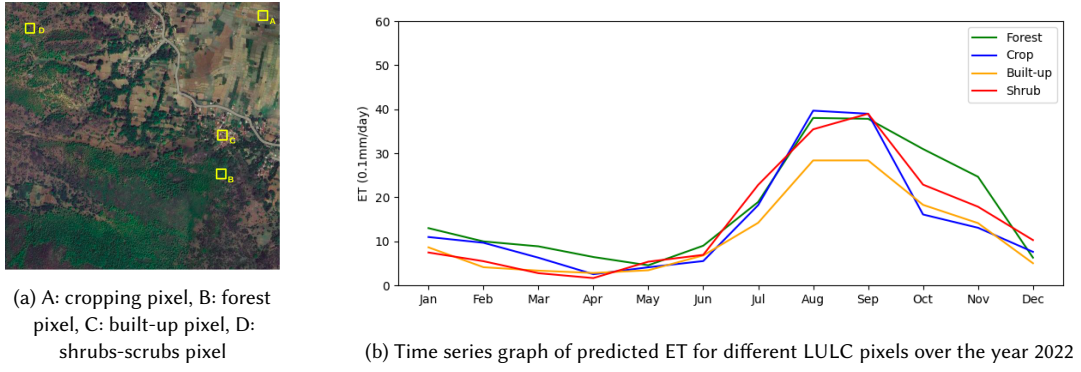


Fig. 9.  $2\text{km} \times 2\text{km}$  region with four  $30\text{m} \times 30\text{m}$  pixels, and the time series of predicted ET over the pixels

Variable	Locations					
	Dantiwada	Jodhpur	Durgapura	New Delhi	Rajkot	Anand
	$N_{tr} = 61, N_t = 15$	$N_{tr} = 59, N_t = 14$	$N_{tr} = 73, N_t = 18$	$N_{tr} = 92, N_t = 23$	$N_{tr} = 77, N_t = 19$	$N_{tr} = 40, N_t = 10$
Intercept	5.6(16.599)	-217.14(165.46)	-54.74(195.34)	-14.08(11.42)	-8.34(3.65)*	64.56(19.94)**
Downscaled ET	0.993(0.45)*	-1.24(1.12)	0.496(0.53)	0.87(0.30)**	0.07(0.11)	-0.93(0.81)
Temperature(C)	-0.2(0.58)	-0.48(0.34)	-0.461*(0.19)	0.549(0.27)*	-0.09(0.11)	-1.79(0.79)*
Humidity	-781.61(822.32)	1251.73(840.77)	793.06(515.43)	-535.1(728.68)	-70.47(178.34)*	-186.58(1276)
Soil Moisture	1.01(0.66)	6.12(4.25)	1.82(4.93)	0.95(0.53)	0.59(0.16)***	1.07(0.92)
Precipitation	0.11(0.2)	-0.19(0.3)	-0.01(0.13)	0.07(0.15)	0.02(0.02)	-0.08(0.14)
RMSE	Before	19.13	17.41	14.73	17.88	4.45
	After	15.76	13.31	9.61	14.43	3.41
NRMSE	Before	0.22	0.366	0.36	0.344	0.28
	After	0.32	0.37	0.27	0.34	0.28
$R^2$	Before	0.14	0.008	0.1537	0.15	0.177
	After	0.12	0.04	0.22	0.17	0.35
Pearson	Before	0.378	0.09	0.392	0.3877	0.421
	After	0.30	0.04	0.43	0.38	0.56
						0.23

Variable	Locations					
	Bhopal	Raipur	Lucknow	AEZ-2	AEZ-4	AEZ-5
	$N_{tr} = 41, N_t = 10$	$N_{tr} = 99, N_t = 24$	$N_{tr} = 106, N_t = 26$	$N_{tr} = 124, N_t = 31$	$N_{tr} = 262, N_t = 65$	$N_{tr} = 40, N_t = 10$
Intercept	43.01(9.52)***	28.52(7.59)***	-2.42(4.56)	15.08(8.73)*	3.95(3.16)	64.56(19.94)*
Downscaled ET	0.84(0.28)*	-0.64(0.25)*	0.46(0.24)*	1.01(0.36)*	0.63(0.15)***	-0.93(0.81)
Temperature(C)	-1.25(0.3)***	-0.32(0.26)	0.3(0.16)*	-0.45(0.31)	-0.04(0.12)	-1.79(0.79)*
Humidity	1960.43(918.62)*	810.27(565.84)	597.45(388.33)	557.57(517.82)	156.08(253.55)	-186.58(1276)
Soil Moisture	-0.69(0.36)*	0.37(0.29)	0.03(0.16)	0.21(0.14)	0.2(0.06)*	1.07(0.92)
Precipitation	-0.14(0.36)	-0.05(0.07)	0.01(0.1)	-0.03(0.16)	0.06(0.04)	-0.08(0.14)
RMSE	Before	14.77	23.88	11.90	19.8	12.7
	After	10.26	10.13	8.07	14.939	10.16
NRMSE	Before	0.27	0.547	0.32	0.266	0.3
	After	0.30	0.29	0.25	0.29	0.25
$R^2$	Before	0.41	0.003	0.13	0.075	0.123
	After	0.49	0.07	0.28	0.11	0.18
Pearson	Before	0.64	-0.06	0.36	0.27	0.35
	After	0.68	0.23	0.51	0.33	0.4
						0.23

Variable	Locations			
	AEZ-9	AEZ-10	AEZ-11	AEZ-13
	$N_{tr} = 38, N_t = 9$	$N_{tr} = 41, N_t = 10$	$N_{tr} = 99, N_t = 24$	$N_{tr} = 106, N_t = 26$
Intercept	35.42 (28.8)	43.01(9.52)***	28.52(7.59)***	-2.42(4.56)
Downscaled ET	2.01(1.23)	0.84(0.28)*	-0.64(0.25)*	0.46(0.24)*
Temperature(C)	0.08(0.81)	-1.25(0.3)***	-0.32(0.26)	0.3(0.16)*
Humidity	-166.62(2321.42)	1,960.43(918.62)*	597.45(388.33)	557.57(517.82)
Soil Moisture	-0.95(1.48)	-0.69(0.36)*	0.37(0.29)	0.03(0.16)
Precipitation	-1.35(3.29)	-0.14(0.36)	-0.05(0.07)	0.01(0.1)
RMSE	Before	17.804	14.77	23.88
	After	32.87	10.26	10.13
NRMSE	Before	0.431	0.276	0.547
	After	0.49	0.3	0.29
$R^2$	Before	0.364	17. 41	0.003
	After	0.03	0.49	0.07
Pearson	Before	0.133	0.64	-0.6
	After	-0.03	0.68	0.23
				0.51

Table 6. Multi-variate Linear Regression Statistics for various locations (Using only FLDAS Variables. Values are of the form "coefficient (Standard Error)".  $N_{tr}$  = Number of training samples;  $N_t$  = Number of test samples; \*:  $0.1 > p \geq 0.01$ ; \*\*:  $0.01 > p \geq 0.001$ ; \*\*\*:  $0.001 > p > 0.0001$

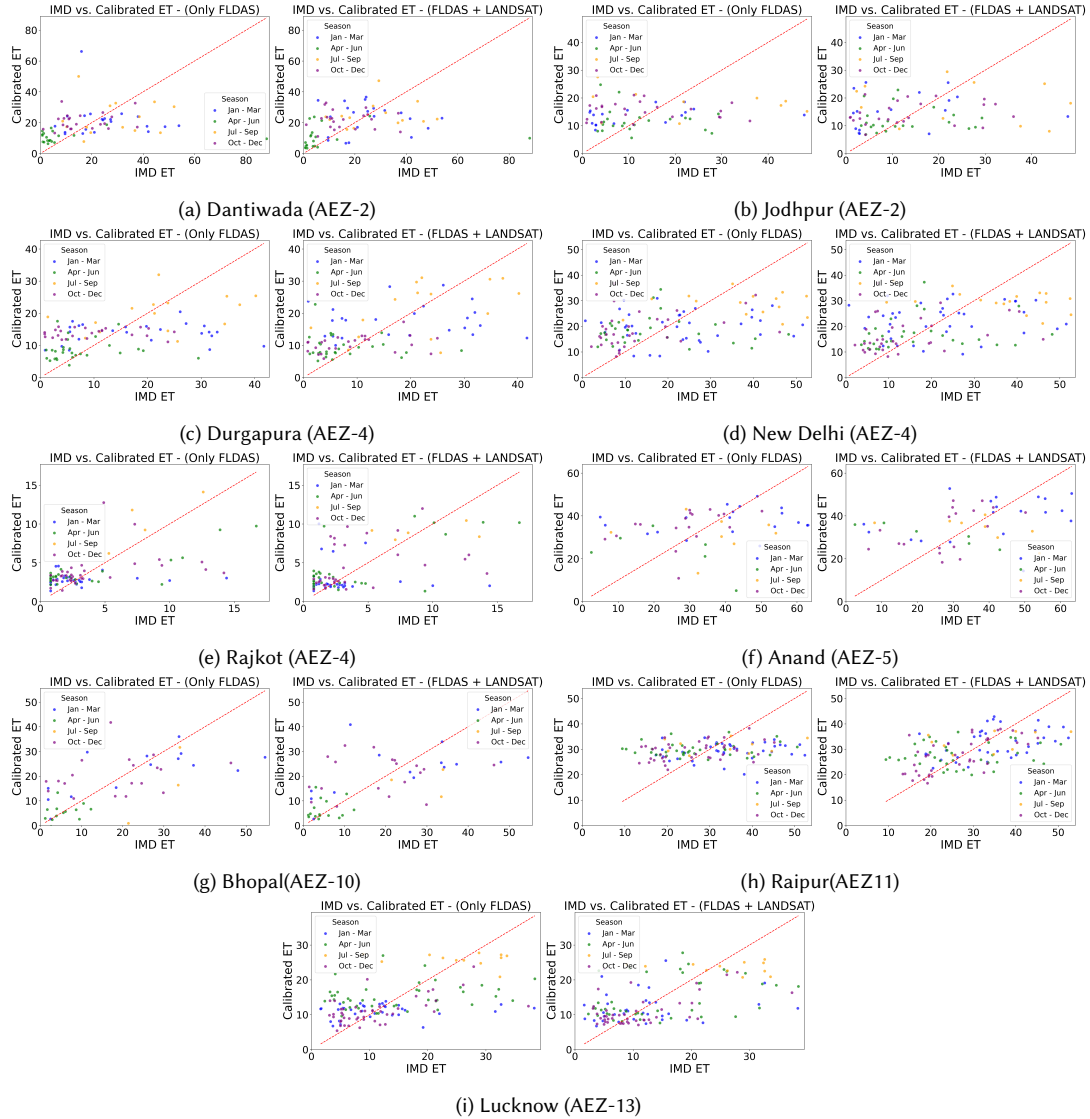


Fig. 10. Graphs for calibrated ET vs IMD (in situ) ET for different locations. Calibration was performed both by only considering FLDAS variables as features (using linear regression) and also FLDAS along with Landsat 7 variables (using random forest).

## 7 CONCLUSION AND FUTURE WORK

In this paper, we demonstrated the usefulness of a Random Forest model for downscaling ET, intended for public use on GEE. Our work represents a significant advance in providing accessible and accurate high-resolution ET estimates for hydro-ecological applications. By providing a finer spatial resolution of ET that provided by several open data products, this methodology can help build a more detailed understanding of ET patterns. We found that the model is adequate to produce relative ET comparisons across different locations at a spatial resolution of  $30m$ , although it is not adequate to match against in situ measurements of actual ET. This may be due to too coarse grained meteorological variables which don't capture fine locational variations, and perhaps also poor quality in situ data. Perhaps one direction to explore further would be to interpolate meteorological data more finely. GEE provides limited functionality for this purpose though, and the alternative of downloading all data for local processing is also challenging. Another gap we identified was the limitation of the model to estimate ET beyond the  $5mm$  range. We found that these cases were mostly over forested areas, and a possible way forward could be to over-sample pixels from these locations, and perhaps to build LULC specific models. These are some directions we plan to pursue in the future.

## 8 ACKNOWLEDGEMENTS

We would like to thank Tower Research, GIZ, and Tarides for supporting the research, Professor Athira P. from IIT Palakkad and Craig Dsouza from WELL Labs for very helpful discussions, and officials from the Indian Meteorological Department (IMD) for providing access to ET measurements.

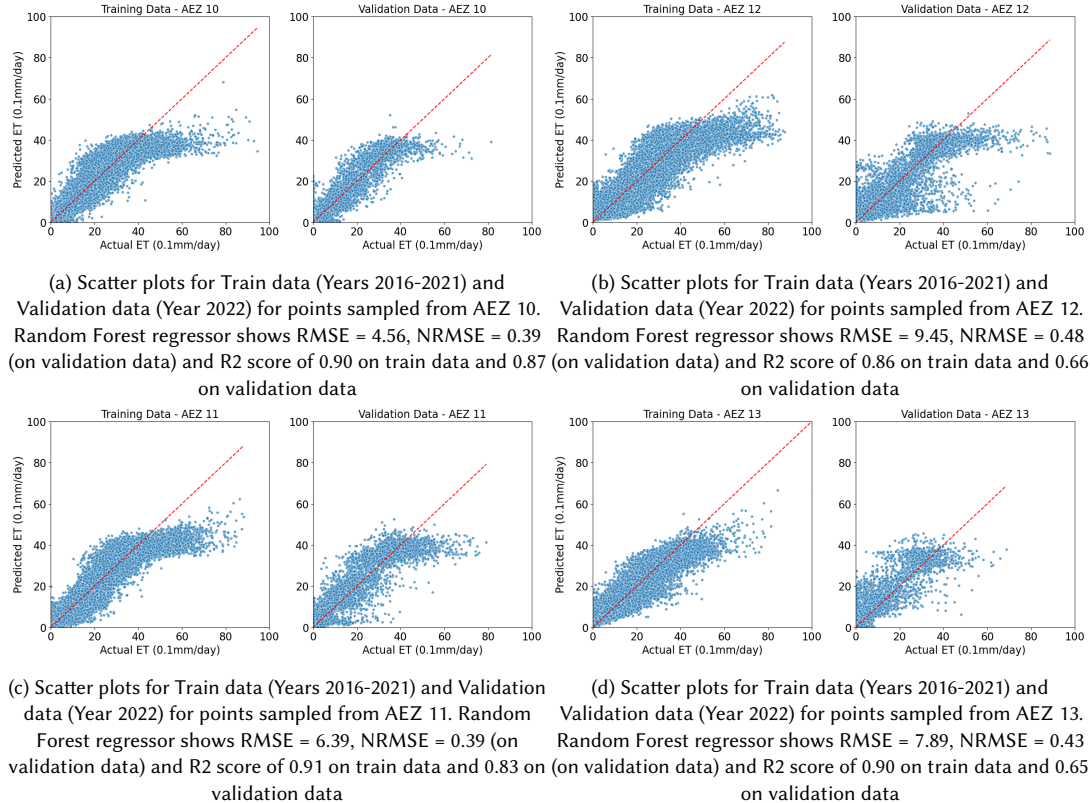


Fig. 11. Scatter plots for training and validation data for the AEZ-wise random forest models. x and y axis show ET in units of 0.1mm/day

## REFERENCES

- [1] Richard Allan, L. Pereira, and Martin Smith. *Crop evapotranspiration-Guidelines for computing crop water requirements-FAO Irrigation and drainage paper 56*. Vol. 56. Jan. 1998.
- [2] H. Beaudoin and M. Rodell. “NASA/GSFC/HSL, GLDAS Noah Land Surface Model L4 3 hourly 0.25 x 0.25 degree V2.1”. In: *Greenbelt, Maryland, USA, Goddard Earth Sciences Data and Information Services Center (GES DISC)* (2020). doi: 10.5067/E7TYRXPJKWQ.
- [3] Ling Bian and Rachel Butler. “Comparing effects of aggregation methods on statistical and spatial properties of simulated spatial data”. In: *Photogrammetric engineering and remote sensing* 65 (1999), pp. 73–84.
- [4] José Da Silva Júnior et al. “Random forest techniques for spatial interpolation of evapotranspiration data from Brazilian’s Northeast”. In: *Computers and Electronics in Agriculture* 166 (Nov. 2019), p. 105017. doi: 10.1016/j.compag.2019.105017.
- [5] T. Davie and N.W. Quinn. *Fundamentals of Hydrology*. Routledge fundamentals of physical geography series. Routledge, 2019. ISBN: 9780415858700. URL: <https://books.google.co.in/books?id=D4b3oAEACAAJ>.
- [6] Indian Meteorological Department. *IMD*. 2024. URL: <https://dsp.imdpune.gov.in/>.
- [7] Arvind Dhaloya et al. “Modeling medium resolution evapotranspiration using downscaling techniques in north-western part of India”. In: *MAUSAM* 74.3 (Jan. 2024), pp. 561–578. doi: 10.54302/mausam.v74i3.5112. URL: <https://mausamjournal.imd.gov.in/index.php/MAUSAM/article/view/5112>.
- [8] Yihun T. Dile et al. “Evaluating satellite-based evapotranspiration estimates for hydrological applications in data-scarce regions: A case in Ethiopia”. In: *Science of The Total Environment* 743 (2020), p. 140702. ISSN: 0048-9697. doi: <https://doi.org/10.1016/j.scitotenv.2020.140702>. URL: <https://www.sciencedirect.com/science/article/pii/S0048969720342248>.
- [9] P. Droogers, W.W. Immerzeel, and I.J. Lorite. “Estimating actual irrigation application by remotely sensed evapotranspiration observations”. In: *Agricultural Water Management* 97.9 (2010), pp. 1351–1359. ISSN: 0378-3774. doi: <https://doi.org/10.1016/j.agwat.2010.03.017>. URL: <https://www.sciencedirect.com/science/article/pii/S0378377410001149>.

- [10] I. Aguado E. Chuvieco D. Riaño and D. Caceres. "Estimation of fuel moisture content from multitemporal analysis of Landsat Thematic Mapper reflectance data: Applications in fire danger assessment". In: *International Journal of Remote Sensing* 23.11 (2002), pp. 2145–2162. doi: 10.1080/01431160110069818. eprint: <https://doi.org/10.1080/01431160110069818>. URL: <https://doi.org/10.1080/01431160110069818>.
- [11] Google Earth Engine. *Landsat*. 2024. URL: [https://developers.google.com/earth-engine/datasets/catalog/LANDSAT\\_LE07\\_C02\\_T1\\_L2](https://developers.google.com/earth-engine/datasets/catalog/LANDSAT_LE07_C02_T1_L2).
- [12] KS Gajbhiye and C Mandal. "Agro-ecological zones, their soil resource and cropping systems". In: *Status of Farm Mechanization in India, cropping systems, status of farm mechanization in India* (2000), pp. 1–32.
- [13] Ikhlas Ghiat, Hamish R. Mackey, and Tareq Al-Ansari. "A Review of Evapotranspiration Measurement Models, Techniques and Methods for Open and Closed Agricultural Field Applications". In: *Water* 13.18 (2021). ISSN: 2073-4441. doi: 10.3390/w13182523. URL: <https://www.mdpi.com/2073-4441/13/18/2523>.
- [14] M.R. Goyal and E.W. Harmsen. *Evapotranspiration: Principles and Applications for Water Management*. Apple Academic Press, 2013. ISBN: 9781926895581. URL: <https://books.google.co.in/books?id=iVHGAAAAQBAJ>.
- [15] Sanayani Hodam et al. "Spatial Interpolation of Reference Evapotranspiration in India: Comparison of IDW and Kriging Methods". In: *Journal of The Institution of Engineers (India): Series A* 98 (Nov. 2017), pp. 511–524. doi: 10.1007/s40030-017-0241-z.
- [16] Taehiee Hwang et al. "Downscaling real-time vegetation dynamics by fusing multi-temporal MODIS and Landsat NDVI in topographically complex terrain". In: *Remote Sensing of Environment* 115.10 (2011), pp. 2499–2512. ISSN: 0034-4257. doi: <https://doi.org/10.1016/j.rse.2011.05.010>. URL: <https://www.sciencedirect.com/science/article/pii/S0034425711001829>.
- [17] *India State of Forest Report* (2021). Tech. rep. Forest Survey of India, Dehradun, 2021.
- [18] Yasir Kaheil et al. "Downscaling and Forecasting of Evapotranspiration Using a Synthetic Model of Wavelets and Support Vector Machines". In: *Geoscience and Remote Sensing, IEEE Transactions on* 46 (Oct. 2008), pp. 2692–2707. doi: 10.1109/TGRS.2008.919819.
- [19] Yinghai Ke et al. "Downscaling of MODIS One Kilometer Evapotranspiration Using Landsat-8 Data and Machine Learning Approaches". In: *Remote Sensing* 8.3 (2016). ISSN: 2072-4292. doi: 10.3390/rs8030215. URL: <https://www.mdpi.com/2072-4292/8/3/215>.
- [20] Yinghai Ke et al. "Downscaling of MODIS One Kilometer Evapotranspiration Using Landsat-8 Data and Machine Learning Approaches". In: *Remote Sensing* 8.3 (2016). ISSN: 2072-4292. doi: 10.3390/rs8030215. URL: <https://www.mdpi.com/2072-4292/8/3/215>.
- [21] D. Kool et al. "A review of approaches for evapotranspiration partitioning". In: *Agricultural and Forest Meteorology* 184 (2014), pp. 56–70. ISSN: 0168-1923. doi: <https://doi.org/10.1016/j.agrformet.2013.09.003>. URL: <https://www.sciencedirect.com/science/article/pii/S016819231300230X>.
- [22] Jin Li and Andrew D. Heap. "Spatial interpolation methods applied in the environmental sciences: A review". In: *Environmental Modelling Software* 53 (2014), pp. 173–189. ISSN: 1364-8152. doi: <https://doi.org/10.1016/j.envsoft.2013.12.008>. URL: <https://www.sciencedirect.com/science/article/pii/S1364815213003113>.
- [23] Muhammad Usman Liaqat et al. "Evaluation of MODIS and Landsat multiband vegetation indices used for wheat yield estimation in irrigated Indus Basin". In: *Computers and Electronics in Agriculture* 138 (2017), pp. 39–47. ISSN: 0168-1699. doi: <https://doi.org/10.1016/j.compag.2017.04.006>. URL: <https://www.sciencedirect.com/science/article/pii/S0168169916310456>.
- [24] Steven P. Loheide and Steven M. Gorelick. "A local-scale, high-resolution evapotranspiration mapping algorithm (ETMA) with hydroecological applications at riparian meadow restoration sites". In: *Remote Sensing of Environment* 98.2 (2005), pp. 182–200. ISSN: 0034-4257. doi: <https://doi.org/10.1016/j.rse.2005.07.003>. URL: <https://www.sciencedirect.com/science/article/pii/S0034425705002191>.
- [25] Thomas R. Loveland and James R. Irons. "Landsat 8: The plans, the reality, and the legacy". In: *Remote Sensing of Environment* 185 (2016). Landsat 8 Science Results, pp. 1–6. ISSN: 0034-4257. doi: <https://doi.org/10.1016/j.rse.2016.07.033>. URL: <https://www.sciencedirect.com/science/article/pii/S0034425716302905>.
- [26] Xiaoliang Lu and Qianlai Zhuang. "Evaluating evapotranspiration and water-use efficiency of terrestrial ecosystems in the conterminous United States using MODIS and AmeriFlux data". In: *Remote Sensing of Environment* 114.9 (2010), pp. 1924–1939. ISSN: 0034-4257. doi: <https://doi.org/10.1016/j.rse.2010.04.001>. URL: <https://www.sciencedirect.com/science/article/pii/S0034425710001124>.
- [27] Qiaozhen Mu, Maosheng Zhao, and Steven W Running. "MODIS global terrestrial evapotranspiration (ET) product (NASA MOD16A2/A3)". In: *Algorithm Theoretical Basis Document, Collection 5* (2013), p. 600.
- [28] R.C. Pipunic, J.P. Walker, and A. Western. "Assimilation of remotely sensed data for improved latent and sensible heat flux prediction: A comparative synthetic study". In: *Remote Sensing of Environment* 112.4 (2008). Remote Sensing Data Assimilation Special Issue, pp. 1295–1305. ISSN: 0034-4257. doi: <https://doi.org/10.1016/j.rse.2007.02.038>. URL: <https://www.sciencedirect.com/science/article/pii/S0034425707003215>.
- [29] Nathaniel P. Robinson et al. "A Dynamic Landsat Derived Normalized Difference Vegetation Index (NDVI) Product for the Conterminous United States". In: *Remote Sensing* 9.8 (2017). ISSN: 2072-4292. doi: 10.3390/rs9080863. URL: <https://www.mdpi.com/2072-4292/9/8/863>.
- [30] Q. Mu Running S. and M. Zhao. "MODIS/Terra Net Evapotranspiration 8-Day L4 Global 500m SIN Grid V061". In: *NASA EOSDIS Land Processes Distributed Active Archive Center* (2021). doi: 10.5067/MODIS/MOD16A2.061.
- [31] NK Shrestha and S Shukla. "Support vector machine based modeling of evapotranspiration using hydro-climatic variables in a sub-tropical environment". In: *Agricultural and forest meteorology* 200 (2015), pp. 172–184.
- [32] RB Smith. "The heat budget of the earth's surface deduced from space". In: *Yale University Center for Earth Observation: New Haven, CT, USA* (2010).
- [33] Famine Early Warning Systems Network (FEWS NET) Land Data Assimilation System. *FLDAS*. 2024. URL: [https://disc.gsfc.nasa.gov/datasets/FLDAS\\_NOAH001\\_G\\_CA\\_D\\_001/summary](https://disc.gsfc.nasa.gov/datasets/FLDAS_NOAH001_G_CA_D_001/summary).
- [34] Alexia Tsouni et al. "Estimation of Actual Evapotranspiration by Remote Sensing: Application in Thessaly Plain, Greece". In: *Sensors* 8.6 (2008), pp. 3586–3600. ISSN: 1424-8220. doi: 10.3390/s8063586. URL: <https://www.mdpi.com/1424-8220/8/6/3586>.

- [35] Emily Wilson and Steven Sader. "Detection of forest harvest type using multiple dates of Landsat TM imagery". In: *Remote Sensing of Environment* 80 (June 2002), pp. 385–396. doi: 10.1016/S0034-4257(01)00318-2.
- [36] Jiangzhou Xia et al. "Satellite-Based Analysis of Evapotranspiration and Water Balance in the Grassland Ecosystems of Dryland East Asia". In: *PLOS ONE* 9.5 (May 2014), pp. 1–11. doi: 10.1371/journal.pone.0097295. URL: <https://doi.org/10.1371/journal.pone.0097295>.
- [37] Hanqiu Xu. "Extraction of Urban Built-up Land Features from Landsat Imagery Using a Thematicoriented Index Combination Technique". In: *Photogrammetric Engineering Remote Sensing* 73 (Dec. 2007), pp. 1381–1391. doi: 10.14358/PERS.73.12.1381.
- [38] B. P. Yadav et al. "Rainfall Statistics of India – 2021". In: *MoES/IMD/HS/Rainfall Report/02(2022)/60* (2021).
- [39] Yang Yong et al. "Estimating evapotranspiration by coupling Bayesian model averaging methods with machine learning algorithms". In: *Environmental Monitoring and Assessment* 193 (Mar. 2021). doi: 10.1007/s10661-021-08934-1.